SIAM J. APPL. MATH.
Vol. 39, No. 3, December 1980

0036-1399/80/3903-0009 $01.00/0

MOTION-INDUCED SINGULARITIES IN POWER SPECTRA ASSOCIATED WITH OCEAN GRAVITY-WAVE FLUCTUATIONS*

E. Y. HARPER†

Abstract. We consider an observer with a measuring device having a scalar output that is linearly related to the random motion of ocean gravity waves. The device could measure waveheight, a component of flow velocity, etc. We study the power-spectral density of the time record obtained when the observer moves at constant speed in a horizontal plane. When the observer is at rest the spectrum is wideband, or incoherent. However when the observer moves, he may move with the envelope of a certain packet of waves, thereby introducing a strong coherence. This coherence manifests itself as a singularity in the power-spectral density of the time record. The location of the singularity in the frequency domain is predicted by the method of stationary phase, but the nature of the singularity is not. It is shown that for the case of swell the spectrum has a square-root singularity on the left, and a finite limit from the right, at the singular point. This peculiar behaviour is demonstrated experimentally. For the case of a wind-driven sea the singularity is logarithmic and unsymmetric about the singular point. For this case the location of the singularity in the frequency domain depends only on the observer's speed, U, and is given by $g/8\pi U$ (cycles/unit time) where g is the acceleration of gravity.

1. Introduction. We consider an observer who is moving horizontally at constant speed in proximity to a random field of linear ocean-surface gravity waves. The observer records the output from a measuring device whose response is linearly related to the local surface-wave motion. The device could be a wavestaff, a flowmeter, or even a magnetometer (see Podney, (1979)). We wish to describe the statistical properties of this record; in particular, we are interested in the power spectral density, $S(\sigma)$, where σ denotes angular frequency. We assume that the measuring device has a transfer function with no sharp peaks, that is, no resonance features within the measurement frequency band. In that case the power spectrum measured when the observer is *at rest* is a smooth continuous function that we would characterize as wideband and incoherent; see for example the waveheight spectrum, $S_{\eta_{1D}}(\omega)$, in App. A. We have used the symbol ω for angular frequency, as distinct from σ, to denote spectra of time records taken by a nonmoving observer.

It is generally the case that when the observer moves there is a strong coherence, that is, a singularity in the spectrum $S(\sigma)$, at a frequency, σ_m, that depends on the observer's speed, U. This is due to the dispersive nature of gravity waves, and is most easily appreciated by first considering all the gravity waves to be moving in the same direction. The waves contained within a narrow band of frequencies, centered at ω_m within the spectrum $S_{\eta_{1D}}(\omega)$, have wavenumbers with magnitudes in a narrow band Γ_m,

$$\Gamma_m = \frac{\omega_m^2}{g},$$

where g is the acceleration of gravity, and have a group speed U_g,

$$U_g = \frac{g}{2\omega_m},$$

in the direction of wave motion. Suppose the observer moves at an angle, α, with respect

* Received by the editors October 10, 1978, and in final revised form January 15, 1980..

† Bell Laboratories, Whippany, New Jersey 07981. Present address: Office of the Chief of Naval Operations, OP-21, Pentagon Building, Washington, D.C. 20350.

to the direction of motion of this "packet" of waves, where

$$|\alpha| < \frac{\pi}{2}$$

and suppose his speed U is

$$U = \frac{U_g}{\cos\alpha} = \frac{g}{2\omega_m \cos\alpha}.$$

Then the observer moves with the envelope of the wave packet; that is, the projection of his velocity in the direction of motion of the wave packet equals the group velocity of the wave packet. In more mathematical terms, the Fourier integral analysis of the above-cited situation reveals a point of stationary phase at $\omega = \omega_m$ where

$$\omega_m = \frac{g}{2U\cos\alpha}.$$

This means that in an asymptotic sense, the observer always *sees* the *same* wavelength and frequency as he moves along with this dispersive wave field (see Lighthill (1978, 3.7)). The interpretation of this asymptotic result with respect to the spectrum, $S(\sigma)$, of a time record taken by the observer, is that there will be a delta function in $S(\sigma)$ at the observer's frequency of encounter, σ_m, with the crests of this wave packet

$$\sigma_m = \frac{\omega_m}{2} = \frac{g}{4U\cos\alpha}.$$

Of course there will also be broadband energy in the spectrum $S(\sigma)$, due to the observer's encounter with all the other wave packets constituting $S_{\eta_{1D}}(\omega)$, with those envelopes he is not moving.

The stationary phase result is asymptotic. The observer does not see *exactly* the *same* wavelength and frequency associated with the wave packet. Rather, the wave packet produces a very narrowband process centered at σ_m and displaying amplitude and phase modulation (see Lighthill (1978, 3.6)). The spectrum $S(\sigma)$ does not have a delta function at σ_m, but it does have an integrable singularity there. The purpose of this paper is to display the nature of that singularity. This is best achieved by computing the spectrum, $S(\sigma)$, exactly.

The ocean surface is generally composed of dispersive waves moving in all directions, ψ. The surface is described in terms of a directional-frequency spectrum, $S_{\eta_{2D}}(\omega, \psi)$ (see Phillips (1969)). The point of stationary phase for the two dimensional Fourier integral analysis is at

$$\psi = \alpha, \quad \omega = \frac{g}{2U}, \quad \sigma = \frac{g}{4U},$$

which means that there is destructive interference among all the waves except for the wave packet moving in the direction of the observer and overtaking him at his own speed. Again, this is an asymptotic result, and the spectrum, $S(\sigma)$, does not manifest perfect coherence (a delta function) at $\sigma = g/4U$. The exact representation for $S(\sigma)$ reveals an integrable singularity at that frequency, but of a type different from the singularity that occurs when all the waves move in the same direction.

The spectrum $S(\sigma)$ is one statistic of the time record taken by the observer. Many processes can have the same spectrum because the relative phase of sinusoids at different frequencies is not specified. Therefore a time series realization of the process

in question is of interest because the "coherence" implied by the singularities in $S(\sigma)$ may be appreciated in another way. For this reason a few theoretical time series realizations are presented. We have chosen to compute the axial component of fluctuating velocity because this quantity could easily be measured by means of a flowmeter aboard a ship at sea.

Finally, the theoretical results have been verified experimentally. This will be the subject of another paper. However, we show here one preliminary result for the following reason. The predicted singularity for the case of waves moving in one direction is quite unusual. It is discontinuous at σ_m, and singular from the left but not from the right. The result for waves in all directions is an integral over this solution. One may well ask whether this mathematical result, based on linear theory, would ever be seen in nature. A preliminary answer has been obtained in the main towing tank at the David Taylor model basin. The tank is 15.2 *m* wide, 549 *m.* long, and 7 *m.* deep, and has a random wave generator at one end with an absorbing beach at the other. The wavemaker generates random finite-amplitude gravity waves, with a prescribed spectrum, for the primary purpose of testing ship slamming. A variable-speed towing carriage runs on rails at a fixed height above the waves for the purpose of towing the models. It was a fairly easy matter to mount an ultrasonic down-looking device on the carriage which could measure the free surface fluctuations with the carriage moving both with and against the waves. The discontinuous singularity from the left in $S_{\eta_{1D}}(\sigma)$, is clearly visible, and is displayed in § 4 of this paper.

2. Problem formulation and derivation of results. We consider an observer with a measuring device who is moving at constant speed U and angle α, in a horizontal plane above or below the ocean surface (see Fig. 1). The observer records the fluctuating scalar output from a measuring device, say a wavestaff or flowmeter, that is linearly

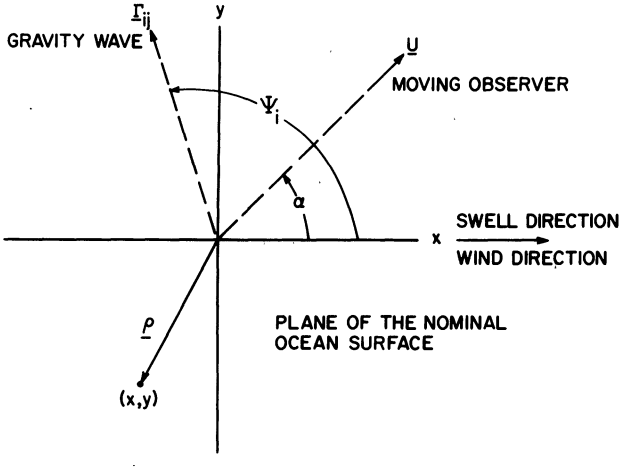

FIG. 1. *A view looking down on the ocean surface. The positive z axis is directed vertically downward.*

related to the random motion of ocean-surface gravity waves. He then forms a power spectrum from this time record. As indicated in the introduction we expect this spectrum to manifest a strong coherence, that is, a singular behavior, for those waves whose projected group velocity, in the direction of the observer's motion, equals the observer's velocity. Our aim is to display the precise nature of this singular behavior.

We consider two cases of a random gravity-wave field. The first case we refer to as a wind-driven sea, with a two-dimensional directional-frequency waveheight spectrum,

$S_{\eta 2 0}(\omega, \psi)$, given by

$$S_{\eta 2 D}(\omega, \psi) = \frac{D(\psi)}{\mathscr{D}} S_{\eta 1 D}(\omega), \tag{1a}$$

where

$$\mathscr{D} = \int_{-\pi}^{\pi} D(\psi)\, d\psi, \tag{1b}$$

and where $S_{\eta 1 D}(\omega)$ is the one-dimensional frequency spectrum (see Phillips (1969)). The wind is assumed to be blowing in the positive x-direction. For the purposes of computation, we choose $S_{\eta 1 D}(\omega)$ to be the Pierson–Moskowitz (1964) frequency spectrum (also see App. A), and $D(\psi)$ to be

$$D(\psi) = \left| \cos \frac{\psi}{2} \right|. \tag{1c}$$

In the second case, which we refer to as the case of swell, the random field is composed of a spectrum of plane gravity waves all moving in the positive x-direction. We treat swell as a special case of a wind-driven sea by setting

$$D(\psi) = \delta(\psi), \qquad \mathscr{D} = 1. \tag{1d}$$

The use of the Pierson–Moskowitz frequency spectrum for the case of swell is a matter of computational convenience. The formulas given in this paper are completely general, and any other one-dimensional waveheight spectrum, $S_{\eta 1 D}(\omega)$, could be used for computations involving the swell case.

The time series from the measuring device has a correlation function, $R(\tau)$, of the general form

$$R(\tau) = \frac{1}{\pi} \int_0^{\infty} \int_{\alpha-\pi}^{\alpha+\pi} G(\omega, \psi, \alpha) S_{\eta 2 D}(\omega, \psi) \cos [\sigma(\omega)\tau]\, d\psi\, d\omega, \tag{2a}$$

where

$$\sigma(\omega) = \omega\left(1 - \frac{\omega}{2\omega_m(\psi)}\right), \tag{2b}$$

$$\omega_m(\psi) = \frac{g}{2U \cos(\psi - \alpha)}, \tag{2c}$$

and g is the acceleration of gravity. The function $G(\omega, \psi, \alpha)$ represents the response of the linear measuring device, e.g., for a wavestaff, whose output is the vertical waveheight, $G = 1$, while for the case of an axial flow meter (see App. A)

$$G = \begin{cases} \cos^2(\psi - \alpha)\omega^2 e^{-2(z/g)\omega^2}, & z > 0, \\ 0, & z < 0. \end{cases} \tag{3}$$

Equation (2) is derived in App. A by constructing realizations of the above-cited random processes as a double sum (over frequency, ω, and direction, ψ) of plane gravity waves with random phases. The correlation function is obtained by ensemble averaging over the random phases and taking the limit as $\Delta\psi$ and $\Delta\omega$ approach zero. The argument $\sigma(\omega)\tau$,

$$\sigma(\omega)\tau = \left[\omega - \frac{\omega^2}{g} U \cos(\psi - \alpha)\right]\tau,$$

arises as follows. A plane gravity wave of frequency ω_j, moving in the direction ψ_i, has the phase (see Fig. 1)

$$\omega_j t - \boldsymbol{\Gamma}_{ij} \cdot \boldsymbol{\rho} + \gamma_{ij},$$

where

$$\boldsymbol{\Gamma}_{ij} = \frac{\omega_j^2}{g}(\cos \psi_i \mathbf{x}_0 + \sin \psi_i \mathbf{y}_0),$$

$\mathbf{x}_0$ and $\mathbf{y}_0$ are unit vectors in the x- and y- directions, and γ_{ij} is a random phase uniformly distributed on the interval $-\pi$ to π. The observer's location is given by $\boldsymbol{\rho}_s$ where

$$\boldsymbol{\rho}_s = Ut(\cos \alpha \mathbf{x}_0 + \sin \alpha \mathbf{y}_0).$$

Substitution of $\boldsymbol{\rho}_s$ for $\boldsymbol{\rho}$ and ensemble averaging on γ_{ij} to obtain the correlation function $R(\tau)$, leads to (see App. A)

$$\left[\omega_j - \frac{\omega_j^2}{g} U \cos(\psi_i - \alpha)\right]\tau.$$

Equation (2) may also be derived by means of a continuous stochastic integral representation of the gravity wave field. Our reason for constructing the realizations in App. A is that the time series themselves are interesting and clearly display the coherence properties implied by the spectra. Some time-series realizations, computed from the formulas in App. A, will be presented at the end of this paper. Our main objective, however, is to display the structure of the singularities in the power spectra. The swell case is treated first; the wind-driven case is then treated as an integral over the solution for swell.

2a. Results for the case of swell. In order to treat the case of swell, we rewrite the kernel of the integral in (2) as

$$G(\omega, \psi, \alpha) S_{\eta 2D}(\omega, \psi) = \frac{D(\psi)}{\mathscr{D}} \kappa(\omega, \psi, \alpha), \tag{4}$$

whence (2) becomes

$$R(\tau) = \frac{1}{\pi \mathscr{D}} \int_{\alpha-\pi}^{\alpha+\pi} \int_0^\infty D(\psi) \kappa(\omega, \psi, \alpha) \cos\left[\omega\left(1 - \frac{\omega}{2\omega_m(\psi)}\right)\right] \tau \, d\omega \, d\psi, \tag{5a}$$

$$\omega_m(\psi) = \frac{g}{2U \cos(\psi - \alpha)}. \tag{5b}$$

The case of swell is then obtained by invoking (1d) whence,

$$R(\tau) = \frac{1}{\pi} \int_0^\infty \kappa(\omega, 0, \alpha) \cos\left[\omega\left(1 - \frac{\omega}{2\omega_m}\right)\right] \tau \, d\omega, \tag{6a}$$

where

$$\omega_m = \frac{g}{2U \cos \alpha}. \tag{6b}$$

This integral has a point of stationary phase or saddle point at $\omega = \omega_m$ when $|\alpha| < \pi/2$. Rather than finding the asymptotic stationary phase approximation to $R(\tau)$, we recast the integral in (6a) so as to display the exact Fourier transform of $R(\tau)$, that is, the power spectrum, $S(\omega)$.

We begin by making the change of variable

$$\sigma = \omega\left(1 - \frac{\omega}{2\omega_m}\right); \tag{7}$$

this function is shown in Fig. 2. In order to compute the Jacobian of the transformation we must consider two cases.

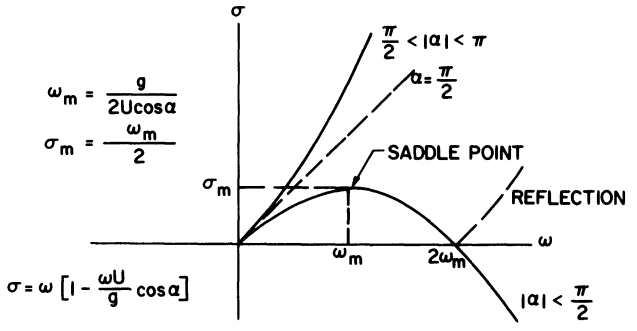

FIG. 2. *The relation between the frequency of encounter with the wavecrests in the moving frame σ, and the frequency in the fixed frame, ω.*

For the case $\omega_m < 0$, the ship moves *against* the waves, that is, $\pi/2 < |\alpha| < \pi$, and there is no saddle point. The functional relation between σ and ω is single valued and we have

$$\omega = -\omega_m\left(\sqrt{1 - \frac{2\sigma}{\omega_m}} - 1\right), \qquad \omega_m < 0, \tag{8a}$$

and

$$d\omega = \frac{d\sigma}{\sqrt{1 - \dfrac{2\sigma}{\omega_m}}}. \tag{8b}$$

The correlation function is then written

$$\mathbf{R}_-(\tau) = \frac{1}{\pi}\int_0^\infty \kappa(N\{\sigma, \sigma_m\}, 0, \alpha)\frac{\cos \sigma\tau}{\sqrt{1 - \dfrac{\sigma}{\sigma_m}}}\, d\sigma \tag{9a}$$

where

$$\omega = N\{\sigma, \sigma_m\} = 2\sigma_m\left(\sqrt{1 - \frac{\sigma}{\sigma_m}} - 1\right), \tag{9b}$$

$$\alpha_m = \frac{\omega_m}{2} = \frac{g}{4U\cos\alpha}, \tag{9c}$$

and the $-$subscript denotes $\sigma_m < 0$. The power spectrum in the moving frame is simply the kernel of the integral in (9a),

$$S(\sigma) = \frac{\kappa(N\{\sigma, \sigma_m\}, 0, \alpha)}{\sqrt{1 - \dfrac{\sigma}{\sigma_m}}}, \qquad \sigma_m < 0. \tag{10}$$

As expected, there are no singularities in the power spectrum $S(\sigma)$.

For the case $\omega_m > 0$, the ship moves *with* the waves, that is $|\alpha| < \pi/2$. The functional relation between σ and ω is multiple valued, and there is a saddle point, or point of stationary phase, at $\omega = \omega_m$. For $0 < \omega < \omega_m$,

$$\omega = 2\sigma_m\left(1 - \sqrt{1 - \frac{\sigma}{\sigma_m}}\right) = M_-\{\sigma, \sigma_m\}, \qquad \sigma_m > 0, \tag{11a}$$

and

$$d\omega = \frac{d\sigma}{\sqrt{1 - \frac{\sigma}{\sigma_m}}}, \tag{11b}$$

while for $\omega_m \leqq \omega$,

$$\omega = 2\sigma_m\left(1 + \sqrt{1 - \frac{\sigma}{\sigma_m}}\right) = M_+\{\sigma, \sigma_m\}, \qquad \sigma_m > 0, \tag{12a}$$

and

$$d\omega = -\frac{d\sigma}{\sqrt{1 - \frac{\sigma}{\sigma_m}}}. \tag{12b}$$

The correlation function for $\omega_m > 0$, denoted $R_+(\tau)$, is

$$\begin{aligned} R_+(\tau) = {} & \frac{1}{\pi}\int_0^{\sigma_m} \kappa(M_-\{\sigma, \sigma_m\}, 0, \alpha) \frac{\cos \sigma\tau}{\sqrt{1 - \frac{\sigma}{\sigma_m}}}\, d\sigma \\ & + \frac{1}{\pi}\int_0^{\sigma_m} \kappa(M_+\{\sigma, \sigma_m\}, 0, \alpha) \frac{\cos \sigma\tau}{\sqrt{1 - \frac{\sigma}{\sigma_m}}}\, d\sigma \\ & + \frac{1}{\pi}\int_0^{\infty} \kappa(M_+\{-\sigma, \sigma_m\}, 0, \alpha) \frac{\cos \sigma\tau}{\sqrt{1 + \frac{\sigma}{\sigma_m}}}\, d\sigma, \end{aligned} \tag{13a}$$

where

$$M_+\{-\sigma, \sigma_m\} = 2\sigma_m\left(1 + \sqrt{1 + \frac{\sigma}{\sigma_m}}\right). \tag{13b}$$

Again the power spectrum is the kernel of the integral in (13a). However, for $\sigma_m > 0$ it is discontinuous at $\sigma = \sigma_m$, and there is a square-root singularity from the left. That is,

$$\begin{aligned} S(\sigma) = {} & \frac{1}{\sqrt{1 - \frac{\sigma}{\sigma_m}}} \{\kappa(M_-\{\sigma, \sigma_m\}, 0, \alpha) + \kappa(M_+\{\sigma, \sigma_m\}, 0, \alpha)\} H\left(1 - \frac{\sigma}{\sigma_m}\right) \\ & + \frac{1}{\sqrt{1 + \frac{\sigma}{\sigma_m}}} \kappa(M_+\{-\sigma, \sigma_m\}, 0, \alpha), \end{aligned} \tag{14}$$

where

$$H\left(1-\frac{\sigma}{\sigma_m}\right)=\begin{cases}1, & \sigma \leqq \sigma_m,\\ 0, & \sigma > \sigma_m.\end{cases}$$

2b. Results for the case of a wind-driven sea. The double integral representation for $R(\tau)$, (5a) and (5b), has a point of stationary phase at

$$\psi=\alpha, \qquad \omega=\frac{g}{2U},$$

(see Felsen and Markuvitz (1973)). The asymptotic representation of the integral picks out the waves moving in the observer's direction with the group velocity equal to the observer's velocity. However, it is not the stationary phase representation for $R(\tau)$ we seek; rather, we seek the exact representation for the power sepctrum $S(\sigma)$.

Inspection of (5a) and (5b) for the wind-driven case, and (6a) and (6b) for the swell case, indicate that the desired result for the wind-driven sea may be obtained as an integral over the result for swell.

For the case of swell, the right-hand side of (6a) was put in the general form

$$R_{\mp}(\tau)=\frac{1}{\pi}\int_0^{\infty}\mathcal{F}_{\mp}[\kappa(\omega\{\sigma,\sigma_m\}0,\alpha),\sigma/\sigma_m]\cos\sigma\tau\,d\sigma \tag{15}$$

where $\mathcal{F}$ denotes a function of κ and σ_m, and the subscripts $-$ and $+$ denote the cases $\sigma_m<0$ and $\sigma_m>0$, respectively (see (9a), (13a)). The argument $\omega\{\sigma,\sigma_m\}$ denotes a member of the set of functions $N\{\sigma,\sigma_m\}$, $M_-\{\sigma,\sigma_m\}$, $M_+\{\sigma,\sigma_m\}$, or $M_+(-\sigma,\sigma_m)$ defined by (9b), (11a), (12a), and (13b), respectively. The expression for the wind-driven case is obtained by replacing $\kappa(\omega\{\sigma,\sigma_m\},0,\alpha)$ with $\kappa(\omega\{\sigma,\sigma_m(\psi)\},\psi,\alpha)$ and σ/σ_m with $\sigma/\sigma_m(\psi)$, and integrating over (ψ). The result is

$$\begin{aligned}\pi R(\tau)=&\left(\int_{\alpha-\pi}^{\alpha-\pi/2}d\psi+\int_{\alpha+\pi/2}^{\alpha+\pi}d\psi\right)\int_0^{\infty}\frac{D(\psi)}{\mathcal{D}}\mathcal{F}_-[\kappa(\omega\{\sigma,\sigma_m(\psi)\},\psi,\alpha),\sigma/\sigma_m(\psi)]\cos\sigma\tau\,d\sigma\\ &+\int_{\alpha-\pi/2}^{\alpha+\pi/2}d\psi\int_0^{\infty}\frac{D(\psi)}{\mathcal{D}}\mathcal{F}_+[\kappa(\omega\{\sigma,\sigma_m(\psi)\},\psi,\alpha),\sigma/\sigma_m(\psi)]\cos\sigma\tau\,d\sigma.\end{aligned} \tag{16}$$

Now, since

$$R(\tau)=\frac{1}{\pi}\int_0^{\infty}S(\sigma)\cos\sigma\tau\,d\sigma,$$

we have

$$\begin{aligned}S(\sigma)=&\frac{1}{\mathcal{D}}\left(\int_{\alpha-\pi}^{\alpha-\pi/2}d\psi+\int_{\alpha+\pi/2}^{\alpha+\pi}d\psi\right)D(\psi)\mathcal{F}_-[\kappa(\omega\{\sigma,\sigma_m(\psi)\},\psi,\alpha),\sigma/\sigma_m(\psi)]\,d\psi\\ &+\frac{1}{\mathcal{D}}\int_{\alpha-\pi/2}^{\alpha+\pi/2}D(\psi)\mathcal{F}_+[\kappa(\omega\{\sigma,\sigma_m(\psi)\},\psi,\alpha),\sigma/\sigma_m(\psi)]\,d\psi,\end{aligned} \tag{17a}$$

where

$$\mathcal{F}_-[\kappa(\omega\{\sigma,\sigma_m(\psi)\}\psi,\alpha),\sigma/\sigma_m(\psi)]=\frac{\kappa(N\{\sigma,\sigma_m(\psi)\},\psi,\alpha)}{\sqrt{1-\dfrac{\sigma}{\sigma_m(\psi)}}}, \tag{17b}$$

and

$$\mathcal{F}_+[\kappa(\psi\{\sigma, \sigma_m(\psi)\}, \psi, \alpha), \sigma/\sigma_m(\psi)]$$

$$= \frac{\kappa(M_+\{-\sigma, \sigma_m(\psi)\}, \psi, \alpha)}{\sqrt{1+\dfrac{\sigma}{\sigma_m(\psi)}}} + \frac{\{\kappa(M_-\{\sigma, \sigma_m(\psi)\}, \psi, \alpha)+\kappa(M_+\{\sigma, \sigma_m(\psi)\}, \psi, \alpha)\}}{\sqrt{1-\dfrac{\sigma}{\sigma_m(\psi)}}} H\left(1-\frac{\sigma}{\sigma_m(\phi)}\right), \tag{17c}$$

and where

$$H\left(1-\frac{\sigma}{\sigma_m(\psi)}\right) = \begin{cases} 1, & \sigma \leqq \sigma_m(\psi), \\ 0, & \sigma > \sigma_m(\psi). \end{cases} \tag{17d}$$

We note that over the range of integration indicated in (17a), $\sigma_m(\psi)$ takes on only negative values, so that the function $\mathcal{F}_-$ is never singular. On the other hand, the range of integration for $\mathcal{F}_+$ is such that $\sigma_m(\psi)$ takes on only positive values. As a consequence part of the integrand, namely the second term on the right-hand side of (17c), is singular when

$$\sqrt{1-\frac{\sigma}{\sigma_m(\psi)}} = \sqrt{1-\frac{4U\sigma}{g}\cos(\psi-\alpha)} = 0, \tag{18a}$$

that is, when

$$\psi = \alpha \pm \cos^{-1}\frac{g}{4U\sigma}. \tag{18b}$$

Of course this is the square-root singularity due to waves moving *with* the ship, that is $|\psi-\alpha|<\pi/2$.

It should be remembered that the integration in (17a) is with respect to ψ, with σ as a parameter. When $\sigma \neq \sigma_0$, the singularity in the integrand is of the square-root type and is integrable. However, when $\sigma = \sigma_0$ the singularity in the integrand is a first-order pole. As a consequence the power spectrum $S(\sigma)$ has a logarithmic singularity at $\sigma = \sigma_0 = g/4U$. The power spectrum is *unsymmetric* about σ_0. The singular behaviour near $\sigma = \sigma_0$ is derived in App. B.

2c. Summary of results. With reference to Fig. 1, the results may be summarized as follows. For the case of a random spectrum of plane gravity waves all moving in the positive x-direction (the case of swell) there is no singularity in the spectrum $S(\sigma)$ when the observer moves *against* the waves, that is when $\pi/2<|\alpha|<\pi$. When the observer moves *with* the waves, that is when $|\alpha|<\pi/2$, the spectrum is discontinuous and has a square-root singularity from the left at

$$\sigma = \sigma_m = \frac{\sigma_0}{\cos\alpha}, \tag{19a}$$

where

$$\sigma_0 = \frac{g}{4U}. \tag{19b}$$

The singularity is created by the packet of waves with oscillation frequency ω (measured

in the fixed frame of reference) given by,

$$\omega = \omega_m = 2\sigma_m = \frac{g}{2U\cos\alpha}.$$

If the observer changes his speed U, or heading α, the frequency α_m of the singularity in the measured spectrum $S(\sigma)$ changes, as does the identity of the packet of waves responsible for the singularity. If a singularity occurs in the swell case it is because the projection of the observer's velocity in the direction of motion of the wave packet equals the group velocity of the packet.

For the case of an angular distribution of gravity waves (the case of a wind-driven sea) the singularity in $S(\sigma)$ occurs at the frequency

$$\sigma = \sigma_0 = \frac{g}{4U}, \tag{20}$$

and is logarithmic. The singularity is due to those packets of waves moving in, and very nearly in, the direction of the observer, with group velocities equal to, and very nearly equal to, the observer's velocity. These waves oscillate with frequencies near ω_0,

$$\omega_0 = \frac{g}{2U},$$

have wavelengths Λ_0 of

$$\Lambda_0 = \frac{8\pi U^2}{g},$$

and move with phase speed U_0 of

$$U_0 = \frac{\omega_0\Lambda_0}{2\pi} = 2U;$$

that is, they move at twice the observer's speed. What the observer *sees* then is a nearly sinusoidal wave overtaking him at a rate equal to his own speed.

The effects predicted herein, including the discontinuous spectrum of (14), exist in nature. This is demonstrated in § 4, where time records are presented of the waveheight measured from a stable carriage moving with and against random waves propagating down the large towing tank at the David Taylor Model Basin. However, we first show some spectra calculated from the equations derived in this section. We also show time-series realizations, based on the formulas derived in App. A, and having the same theoretical spectra.

3. Spectra and time series. Equations (3), (10), and (14) have been used to calculate the power spectrum of the axial component of fluctuating velocity for the case of swell. Figs. 3 and 4 are for headings of $\alpha = 3\pi/4$ and $\alpha = \pi/4$ respectively. The depth, windspeed and ship speed (observer's speed) are shown on the figures. The windspeed enters through the ocean-surface spectrum $S_{\eta_{1D}}(\omega)$ (see App. A.) Time series realizations for the same directions and values of the parameters are shown in Figs. 5 and 6. The coherence implied by the square-root singularity of Fig. 4 is clearly visible in Fig. 6.

Equations (3) and (17) have been used to calculate the power spectrum of the axial component of fluctuating velocity for the case of a wind-driven sea and a ship's heading of $\alpha = 0$. The results are shown in Fig. 7 along with the values of depth, windspeed and ship speed. The logarithmic singularity at the frequency $g/8\pi U$ (Hz) is clearly visible.

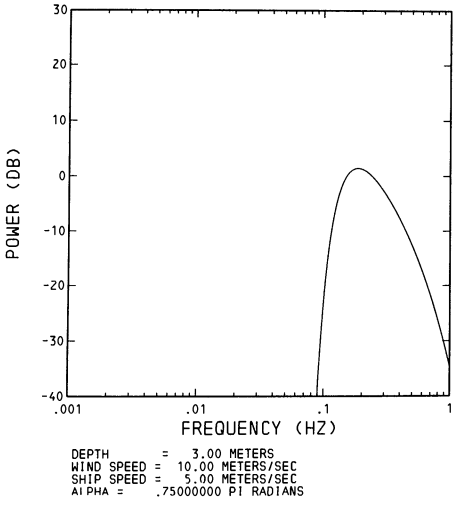

FIG. 3. *The power-spectral density for the axial component of fluctuating velocity. The observer is moving* against *the swell.*

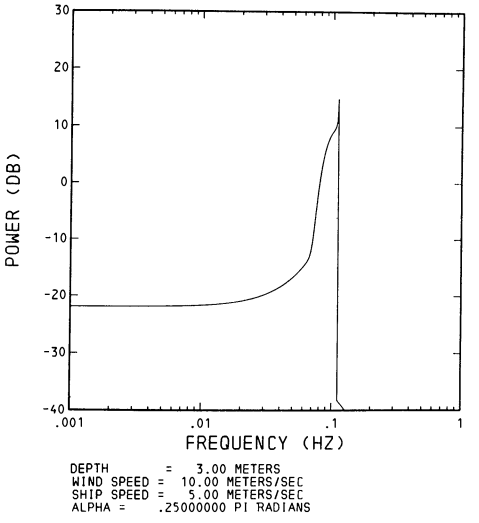

FIG. 4. *The power-spectral density for the axial component of fluctuating velocity. The observer is moving* with *the swell.*

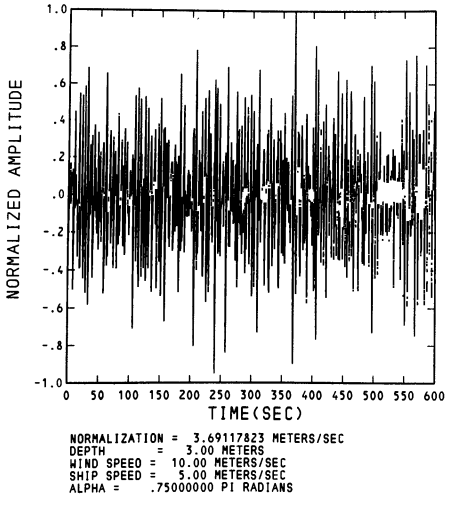

FIG. 5. *A time-series realization for the axial component of fluctuating velocity. The observer is moving* against *the swell. The parameters are those of Fig. 3.*

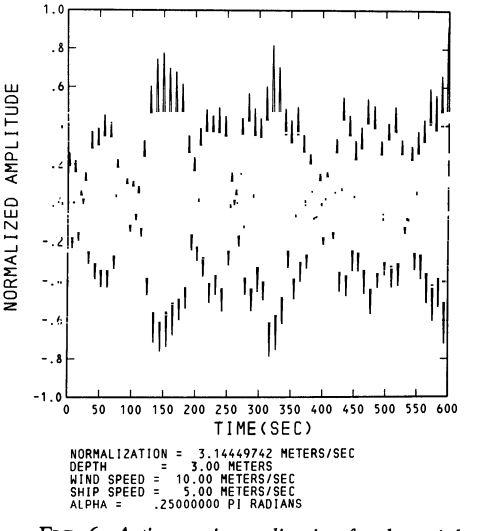

FIG. 6. *A time-series realization for the axial component of fluctuating velocity. The observer is moving* with *the swell. The parameters are those of Fig. 4.*

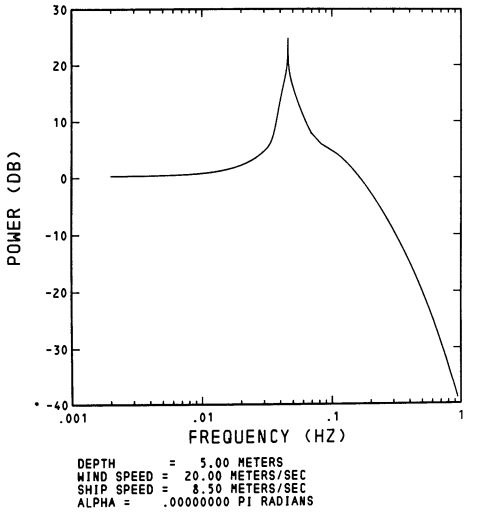

FIG. 7. *The power-spectral density for the axial component of fluctuating velocity. The observer is moving with the wind in a wind-driven sea.*

4. Experimental result. The main towing tank at the David Taylor model basin is approximately 15.2 m (50 ft) wide, 549 m (1800 ft) long, and 7 m (23 ft) deep. At one end, a computer driven pneumatic wave maker can produce waves with a predetermined spectrum. At the other end, an absorbing beach reduces the reflection of waves. The aim is to create one-dimensional, unidirectional surface waves with a prescribed spectrum. In practice, a small amount of energy is reflected by the beach and the tank sides, causing the wave spectrum to vary slightly down the length of the tank.

An instrumentation carriage spans the width of the tank. The carriage is normally used to tow model ships and can move at speeds up to 8.2 m/sec (16 knots). The presence of a beach and the starting and stopping distances for the carriage limit the usable length of the tank from 366 to 457 m (1200 to 1500 ft).

An ultrasonic device, which did not affect the free surface motion, was mounted on the carriage so as to measure the fluctuations in vertical waveheight with the carriage moving against the waves and with the waves. The power in the wavemaker was adjusted slightly below the threshold where there was wave breaking (there was occasional wave breaking during the experiment). The peak in the waveheight spectrum, $S_{\eta_{1D}}(\omega)$, measured with the carriage at rest, corresponded to wavelengths of about 10 feet. The maximum vertical excursion of the surface, peak to trough, was about 1 foot.

If Fig. 8 we present 270 sec of the waveheight time record for the carriage moving 4 feet per second *against* the waves. In Fig. 9 we present 270 sec of the time record for the carriage moving 4 feet per second *with* the waves and with the wavemaker still running at the same setting. The coherence is clearly visible from the record, as it was to observers looking at the waves from the carriage. Observers on the carriage could *see* that as the carriage speed was adjusted from small to larger values in successive tests, this coherent wave appeared to overtake the carriage at higher speeds, until speeds were reached where there was no longer energy in the spectrum.

In Figs. 10 and 11 we present raw spectral estimates (2 degrees of freedom) of the time records of Figs. 8 and 9, respectively. Each spectrum was computed using 320 sec

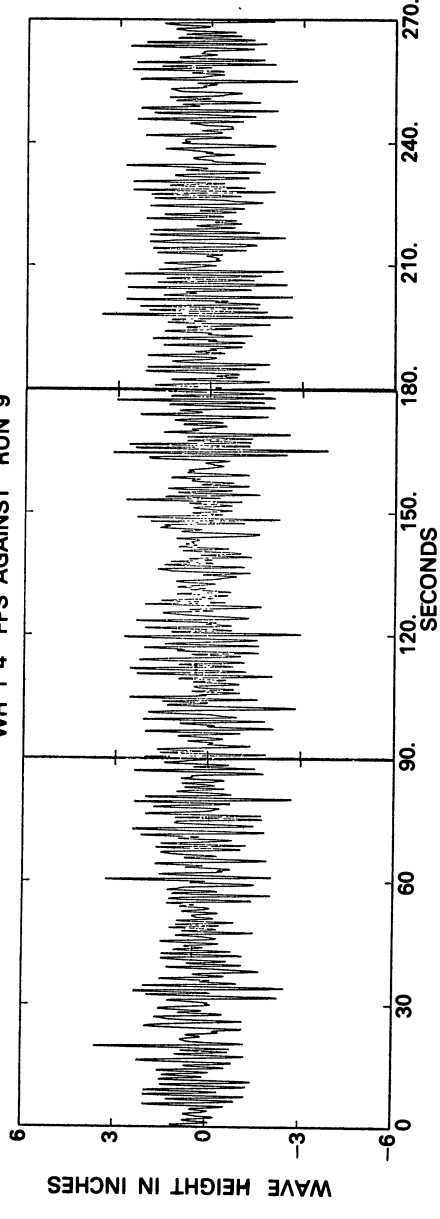

FIG. 8. *Experimental record of the waveheight fluctuations about the mean surface in the David Taylor towing tank. The observer is moving* against *the waves.*

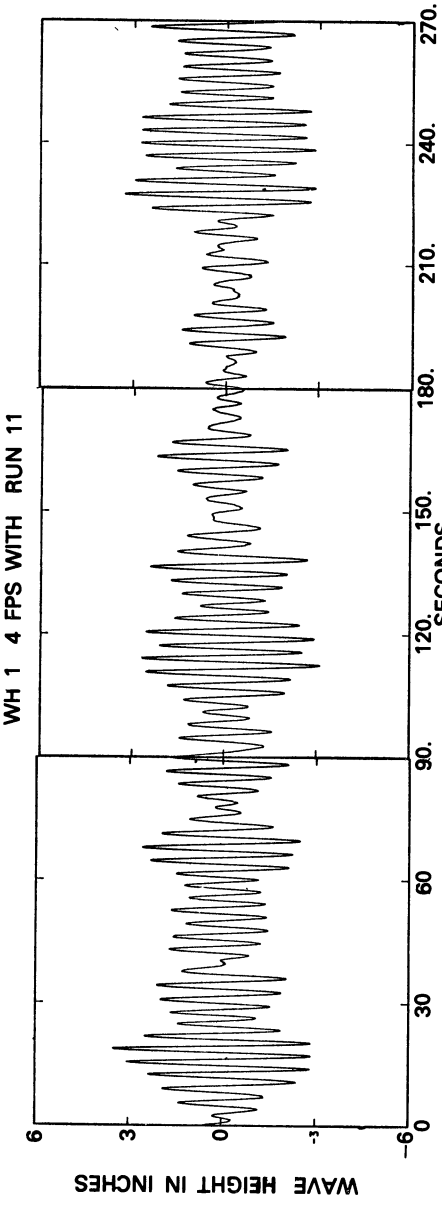

FIG. 9 *Experimental record of the waveheight fluctuations about the mean surface in the David Taylor towing tank. The observer is moving* with *the waves.*

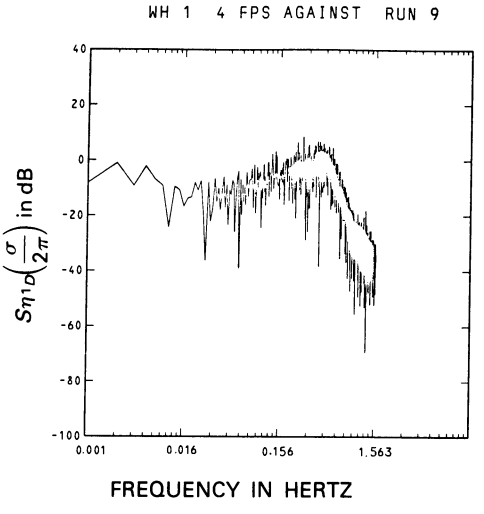

FIG. 10. *The raw spectral estimate of the time series shown in Fig.* 8 *using* 320 *sec. of data. The observer is moving* against *the waves.*

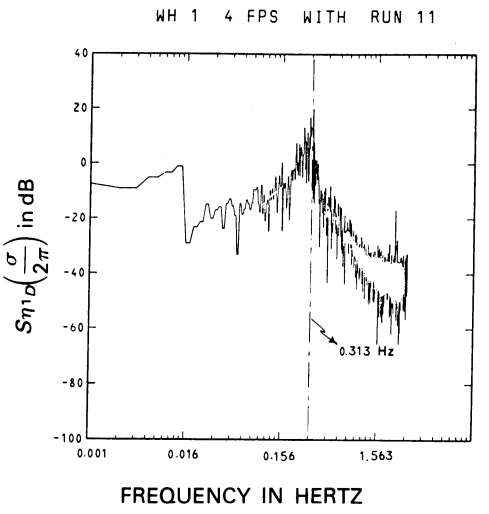

FIG. 11. *The raw spectral estimate of the time series shown in Fig.* 9 *using* 320 *sec. of data. The observer is moving* with *the waves.*

of data (the portions of the record when the carriage was near the wavemaker and the beach were discarded) without any smoothing.

The predicted discontinuity, and singularity from the left, associated with a carriage speed of 4 feet per second, is at

$$f_m = \frac{\sigma_m}{2\pi} = \frac{g}{8\pi U} = 0.32 \text{ Hz}.$$

The largest Fourier coefficient computed from the experiment was at 0.313 Hz. At a frequency 0.01 Hz higher than this, the spectrum had dropped by over 19 dB.

The time series of Fig. 9 is a realization taken from an ensemble. Our definition of power spectrum involves an average over that ensemble (see App. A). One may well ask what, if any, relation this definition of power spectrum bears to the energy measured by means of a finite time record of a single realization, i.e., the spectral estimate of Fig. 11. That is, can we appeal to the usual ergodic principle to relate the ensemble and time averages? There is reason for concern here, particularly with respect to the estimation of the power spectrum in a moving frame and in a narrow frequency band around $\sigma = \sigma_m$. The description of the simplest one-dimensional example of dispersion, given in most texts on waves, serves to illustrate this concern. Consider the addition of two plane sinusoidal gravity waves of equal amplitude but of slightly different wave number, moving in the same direction. An observer moving in the wave direction with the speed of the envelope (group speed) would measure a perfectly coherent signal, but the power in that signal would depend on which point on the envelope the observer follows. For example, the phases of the two waves could be such that the observer moved forever with a null in the envelope in one realization and moved (forever) with a maximum in the envelope in another realization. This is certainly not an ergodic process!

The answer to the above-cited question has been obtained, but the analysis is beyond the scope of this report and will be presented in a subsequent paper. The results are merely summarized here. It is well known that, away from the singularity, the equivalent number of degrees of freedom of a spectral estimate is given by twice the

time bandwidth product. The effect of a square-root singularity in the spectrum is to slightly modify this formula, at least for the case of a stationary Gaussian process. In effect, the continuum of frequencies near $\sigma = \sigma_m$ destroys the strict coherence of the two-wave example as well as the concept of moving with a point of constant amplitude of the envelope. Power spectra obtained from successive runs in the towing tank, and having the same parameter values, may be averaged to increase the confidence in the spectral estimate (degrees of freedom), and improve the signal to noise ratio. These results will also be presented in the paper to follow.

5. Acknowledgment and dedication. I wish to acknowledge the assistance of Drs. Bruce Bogert, Al Claus, Gerald Grube, and Gary Deem, of Bell Laboratories, in the development of these results. I also wish to acknowledge Mr. Ralph Skelly for his computer programming assistance. Most important, I wish to dedicate this paper to my late wife who, despite her illness, encouraged me to continue this research.

Appendix A. We begin by constructing mathematical realizations of the random processes of interest. We choose a Cartesian (x, y, z) coordinate system such that the positive z axis is directed vertically downward and the horizontal $x-y$ plane is coincident with the mean (undisturbed) ocean surface (see Fig. 1). For the case of swell (gravity waves in the frequency band all progressing in a single direction) the direction of propagation is taken to be that of the positive x axis. For the case of wind-driven gravity waves (waves progressing in all directions) the wind is assumed to be blowing in the positive x direction. The ocean surface, $\eta(\boldsymbol{\rho}, t)$, and the fluid velocity potential, $\phi(\boldsymbol{\rho}, z, t)$, (the vector $\boldsymbol{\rho}$ denotes the point x, y in the plane $z = 0$) are assumed to satisfy the steady-state equations of linear invicid gravity-wave theory

$$\left.\begin{aligned} \frac{\partial \eta}{\partial t} &= \frac{\partial \phi}{\partial z} \quad \text{(A1)} \\ g\eta &= \frac{\partial \phi}{\partial t} \quad \text{(A2)} \end{aligned}\right\} \quad \text{on } z = 0,$$

where g is the acceleration of gravity. For the purpose of computing realizations the ocean-surface is constructed as a (double) sum of gravity waves over frequency (index j) and direction (index i), with amplitudes h_{ij} and random phases γ_{ij}. The phases are taken to be statistically independent and uniformly distributed on the interval $-\pi$ to π,

$$\eta(\boldsymbol{\rho}, t) = \sum_{i=1}^{N} \sum_{j=1}^{M} h_{ij} \cos(\boldsymbol{\Gamma}_{ij} \cdot \boldsymbol{\rho} - \omega_j t + \gamma_{ij}). \quad \text{(A3)}$$

The gravity waves oscillate with frequency ω_j, have a wave-number Γ_j given by the dispersion relation

$$\Gamma_j = |\boldsymbol{\Gamma}_{ij}| = \frac{\omega_j^2}{g}, \quad \text{(A4)}$$

and propagate at an angle ψ_i, $-\pi \leqq \psi_i \leqq \pi$, with respect to the positive x axis,

$$\boldsymbol{\Gamma}_{ij} = \frac{\omega_j^2}{g}(\cos \psi_i \mathbf{x}_0 + \sin \psi_i \mathbf{y}_0). \quad \text{(A5)}$$

In (2c), $\mathbf{x}_0$ and $\mathbf{y}_0$ are unit vectors along the positive coordinate axes in the (xyz) frame, which is fixed in space, i.e.,

$$\boldsymbol{\rho} = (x\mathbf{x}_0 + y\mathbf{y}_0). \quad \text{(A6)}$$

The associated potential function that satisfies (A1) and (A2) is

$$\phi(\boldsymbol{\rho}, z, t) = -\sum_{i=1}^{N}\sum_{j=1}^{M} \frac{h_{ij}\omega_j}{\Gamma_j} e^{-\Gamma_j z} \sin(\boldsymbol{\Gamma}_{ij}\cdot\boldsymbol{\rho} - \omega_j t + \gamma_{ij}). \tag{A7}$$

We consider a continuous (in time) point measurement made by an observer moving in a ship at constant velocity $\mathbf{U}$ in a horizontal frame at an angle α with the x axis (see Fig. 1.) The observer's location is given by

$$\boldsymbol{\rho}_s = Ut(\cos\alpha\,\mathbf{x}_0 + \sin\alpha\,\mathbf{y}_0). \tag{A8}$$

Suppose the observer to be measuring the fluctuating component of water speed, relative to the ship, by means of a flowmeter directed along the longitudinal axis of the ship at a depth z below the mean surface. The fluctuating component of water speed relative to the ship is created by the surface-wave motion. The horizontal water velocity measured in the fixed frame, $\mathbf{V}$, is obtained from (A7),

$$\mathbf{V}(\boldsymbol{\rho}, z, t) = \nabla_{\boldsymbol{\rho}}\phi = \sum_{i=1}^{N}\sum_{j=1}^{M} h_{ij}\omega_j e^{-(\omega_j^2/g)z} \frac{\boldsymbol{\Gamma}_{ij}}{\Gamma_j} \cos(\boldsymbol{\Gamma}_{ij}\cdot\rho - \omega_j t + t\gamma_{ij}). \tag{A9}$$

The scalar component of $\mathbf{V}$ in the ship direction and measured at the ship is

$$\hat{u}(\boldsymbol{\rho}_s, z, t) = \sum_{i=1}^{N}\sum_{j=1}^{M} h_{ij}\cos(\psi_i - \alpha)\omega_j e^{-(\omega_j^2/g)z} \cdot\cos\left[\frac{\omega_j^2}{g} Ut\cos(\psi_i - \alpha) - \omega_j t + \gamma_{ij}\right]. \tag{A10}$$

We compute the correlation function by taking the ensemble average over γ_{ij}. The result for $\hat{u}(\boldsymbol{\rho}_s, z, t)$ is

$$R_{\hat{u}}(\tau) = \tfrac{1}{2}\sum_{i=1}^{N}\sum_{j=1}^{M} h_{ij}^2\cos^2(\psi_i - \alpha)\omega_j^2 e^{-2(\omega_j^2/g)z}\cos\sigma_{ij}\tau, \tag{A11}$$

where

$$\sigma_{ij} = \omega_j\left[1 - \frac{\omega_j U}{g}\cos(\psi_i - \alpha)\right]. \tag{A12}$$

In order to render the simulation of the ocean surface ergodic with respect to its mean and correlation function, the amplitudes h_{ij} are chosen in accord with the method of Shinozuka and Jan (1972). The aim is to have the one-dimensional frequency power spectrum of the simulated ocean surface, $S_{\eta_{1D}}(\omega)$ coincide with that of a *real* measured spectrum $S_{\eta_0}(\omega)$, say that of Pierson and Moskowitz (1964). The procedure for calculating the appropriate amplitudes is outlined herein for the case where the directional frequency spectrum to be approximated, $S_{\eta_{2D}}(\omega, \psi)$, has a product form.

We wish to compute the h_{ij} of (A3) so as to simulate a real ocean surface with directional frequency spectrum given by (2), which allows the separation

$$h_{ij} = h_i h_j. \tag{A13}$$

We choose for $S_{\eta_0}(\omega)$ the Pierson–Moscowitz (1964) frequency spectrum,

$$S_{\eta_0}(\omega) = (0.00.81)\frac{\pi g^2}{|\omega^5|} e^{-0.74(g/W\omega)^4} \frac{(m^2)}{(\text{rad/sec})}, \qquad -\infty < \omega < \infty, \tag{A14}$$

where W is the wind speed in (m/sec) (see Fig. A1). The mean square wavelength is

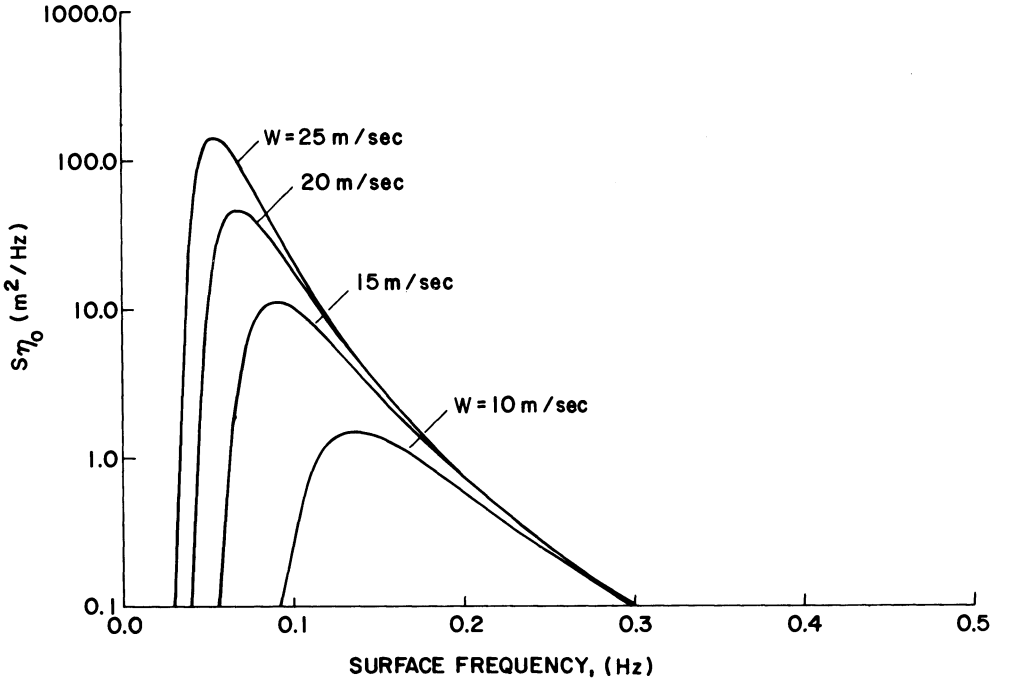

FIG. A1. *The one-dimensional Pierson-Moskowitz frequency spectrum of the ocean surface for various values of the wind speed W.*

given by

$$\sigma_{\eta_0}^2 = \frac{1}{2\pi}\int_{-\infty}^{\infty} S_{\eta_0}(\omega)\, d\omega = \frac{1}{2\pi}\int_{-\infty}^{\infty}\int_{-\pi}^{\pi} S_{\eta_0}(\omega, \psi)\, d\psi\, d\omega. \tag{A15}$$

The one-dimensional frequency power spectrum associated with (A3) is obtained by taking the ensemble average,

$$R_\eta(\tau) = E[\eta(\boldsymbol{\rho}, t)\eta(\boldsymbol{\rho}, t+\tau)], \tag{A16}$$

forming the Fourier transform

$$S_{\eta_{2D}}(\omega, \psi) = \int_{-\infty}^{\infty} R_\eta(\tau)\, e^{i\omega t}\, d\tau = 2\int_0^{\infty} R_\eta(\tau)\cos\omega\tau\, d\tau, \tag{A17}$$

and integrating over ψ,

$$S_{\eta_{1D}}(\omega) = \int_{-\pi}^{\pi} S_{\eta_{2D}}(\omega, \psi)\, d\psi; \tag{A18}$$

the result is

$$S_{\eta_{1D}}(\omega) = \frac{\pi}{2}\sum_{i=1}^{N}\sum_{j=1}^{M} h_i^2 h_j^2 \delta(|\omega| - \omega_j). \tag{A19}$$

We now define

$$\Delta\psi = \frac{2\pi}{N},$$
$$\psi_i = (i-1)\,\Delta\psi, \qquad i = 1, 2, \ldots, N, \tag{A20}$$

and

$$h_i^2 = D(\psi_i)\,\Delta\psi,$$

where $D(\psi)$ is defined by (1).

Equation (A14) is then written

$$S_{\eta_{1D}}(\omega) = \frac{\pi}{2}\left(\sum_{i=1}^{N} D(\psi_i)\,\Delta\psi\right)\sum h_j^2\,\delta(|\omega| - \omega_j). \tag{A21}$$

We choose N sufficiently large so that

$$\left(\sum_{i=1}^{N} D(\psi_i)\,\Delta\psi\right) \approx \int_{-\pi}^{\pi} D(\psi)\,d\psi = \mathscr{D}. \tag{A22}$$

Henceforth we shall denote the sum in (A16) and (A17) by $\mathscr{D}$.

The frequency spectrum of (A9) is nearly band limited between the frequencies $\omega_{\min}$ and $\omega_{\max}$, which depend on the wind speed W, (see Fig. A1). We define the frequency interval

$$\Delta\omega = \frac{\omega_{\max} - \omega_{\min}}{M}, \tag{A23}$$

and the discrete frequencies ω_j,

$$\omega_j = \omega_{\min} + (j - \tfrac{1}{2})\,\Delta\omega + \delta\omega_j, \qquad j = 1, 2, \ldots, M, \tag{A24}$$

where the $\delta\omega j$ are statistically independent random variables uniformly distributed between $-\Delta\omega/L$ and $\Delta\omega/L$ where $L \gg 1$. The continuous spectral density, (A9), is then discretized by concentrating the power in each narrow frequency band $\Delta\omega$ at the associated frequency ω_j, the frequency spectrum then has the form of (A16) where

$$h_j^2 = \frac{2}{\pi\mathscr{D}}\,S_{\eta_0}(\omega_j)\,\Delta\omega. \tag{A25}$$

The purpose in introducing the random frequency perturbations $\delta\omega_j$ in the definition of ω_j, in (A19), is to preclude the possibility of periodicity in time in the simulation of $\eta(\boldsymbol{\rho}, t)$, in (A3). Without these perturbations the representation, (A3), is ergodic with respect to the correlation function. The introduction of the $\delta\omega_j$ renders the stimulation approximately ergodic with respect to $R_{\eta_s}(\tau)$.

Shinozuka and Jan (1972), have shown that the autocorrelation function of the simulated surface, $R_\eta(\tau)$, approaches the autocorrelation function of the real surface, $R_{\eta_0}(\tau)$, as $1/M^2$ for $M \to \infty$. Also, by virtue of the central limit theorem, the simulated surface $\eta(\boldsymbol{\rho}, t)$ approaches a Gaussian process as $M \to \infty$.

Appendix B. As pointed out in § 2, the solution for $S(\sigma)$ in the wind-driven case involves an integration over the angle ψ of the solution for swell, $D(\psi) = \delta(\psi)$. Part of the integrand in (17), namely the second term on the right hand side of (17c), is singular.

In order to investigate the effect of the singularity on $S(\sigma)$ we isolate the singular part of the integral in (17c), $S_s(\sigma)$,

$$S_s(\sigma) = \frac{1}{\mathscr{D}}\int_{\alpha-\pi/2}^{\alpha+\pi/2} D(\psi)\,\frac{[\kappa(M_-\{\sigma, \sigma_m(\psi)\}, \psi, \alpha) + \kappa(M_+\{\sigma, \sigma_m(\psi)\}, \psi, \alpha)]}{\sqrt{1 - \dfrac{\sigma}{\sigma_m(\psi)}}} \cdot H\left(1 - \frac{\sigma}{\sigma_m(\psi)}\right) d\psi. \tag{B1}$$

Because of the step function H, the integral for $S_s(\sigma)$ has two representations depending on whether σ is less than or greater than σ_0. Since

$$1-\frac{\sigma}{\sigma_m(\psi)}=1-\frac{\sigma}{\sigma_0}\cos(\psi-\alpha), \tag{B2}$$

we have for $\sigma<\sigma_0$,

$$S_s(\sigma)\underset{\sigma<\sigma_0}{=}\frac{1}{\mathscr{D}}\int_{\alpha-\pi/2}^{\alpha+\pi/2}D(\psi)\frac{[\kappa(M_-\{\sigma,\sigma_M(\psi)\},\psi,\alpha)+\kappa(M_+\{\sigma,\sigma_m(\psi)\},\psi,\alpha)]}{\sqrt{1-\frac{\sigma}{\sigma_0}\cos(\psi-\alpha)}}\,d\psi, \tag{B3}$$

and for $\sigma>\sigma_0$,

$$S_s(\sigma)\underset{\sigma>\sigma_0}{=}\frac{1}{\mathscr{D}}\left(\int_{\alpha-\pi/2}^{\alpha-\cos^{-1}(\sigma_0/\sigma)}d\psi+\int_{\alpha+\cos^{-1}(\sigma_0/\sigma)}^{\alpha+\pi/2}\right)D(\psi)$$

$$\cdot\frac{[\kappa(M_-\{\sigma,\sigma_m(\psi)\},\psi,\alpha)+\kappa(M_+\{\sigma,\sigma_m(\psi)\},\psi,\alpha)]}{\sqrt{1-\frac{\sigma}{\sigma_0}\cos(\psi-\alpha)}}\,d\psi. \tag{B4}$$

Under the change of variable $\psi-\alpha=\cos^{-1}x$, (B1) becomes

$$S_s(\sigma)\underset{\sigma<\sigma_0}{=}\frac{1}{\mathscr{D}}\int_0^1\left\{D(\alpha+\theta)\left[\kappa\left(M_-\left\{\sigma,\frac{\sigma_0}{x}\right\},\alpha+\theta,\alpha\right)+\kappa\left(M_+\left\{\sigma,\frac{\sigma_0}{x}\right\},\alpha+\theta,\alpha\right)\right]\right.$$

$$\left.+D(\alpha-\theta)\left[\kappa\left(M_-\left\{\sigma,\frac{\sigma_0}{x}\right\},\alpha-\theta,\alpha\right)+\kappa\left(M_+\left\{\sigma,\frac{\sigma_0}{x}\right\},\alpha-\theta,\alpha\right)\right]\right\} \tag{B5}$$

$$\cdot\left[\left(1-\frac{\sigma}{\sigma_0}x\right)(1-x)(1+x)\right]^{-1/2}dx,$$

where

$$\theta=\cos^{-1}x. \tag{B6}$$

The integrand in (B5) has a first-order pole at $x=1$ when $\alpha=\sigma_0$. We remove the singularity by taking the limit of the integrand for $x\to 1$ with $\sigma/\sigma_0<1$ a fixed parameter. We subtract this limit from the integrand of the integral in (B5), and then add the integral of the limit as a second integral; the sum of the two integrals is identical with the integral of (B6). The first integral is now convergent at $x=1$ and is regular as $\sigma\to\sigma_0$. The second integral is singular at $x=1$ and contains the singular behavior of $S_s(\sigma)$ as $\sigma\to\sigma_0$ from the left. The singular part is

$$S_s(\sigma)\underset{\substack{\sigma<\sigma_0\\ \sigma\to\sigma_0}}{\sim}\sqrt{2}D(\alpha)[\kappa(M_-\{\sigma,\sigma_0\},\alpha,\alpha)+\kappa(M_+\{\sigma,\sigma_0\},\alpha,\alpha)]\mathscr{I}_{\sigma<\sigma_0}, \tag{B7}$$

where

$$\mathscr{I}\underset{\sigma<\sigma_0}{=}\int_0^1\left[\frac{\sigma}{\sigma_0}x^2-\left(1+\frac{\sigma}{\sigma_0}\right)x+1\right]^{-1/2}dx$$

$$=\sqrt{\frac{\sigma}{\sigma_0}}\ln\frac{\frac{\sigma}{\sigma_0}-1}{\left[2\sqrt{\frac{\sigma}{\sigma_0}}-\frac{\sigma}{\sigma_0}-1\right]}. \tag{B8}$$

The argument of the logarithm in (B8) is always positive for $\sigma < \sigma_0$ and is zero when $\sigma = \sigma_0$. Under the assumption that the coefficient of $\mathcal{J}_{\sigma<\sigma_0}$ in (B7) is slowly varying and regular as $\sigma \to \sigma_0$, the singular behavior of $S(\sigma)$ from the left is,

$$S(\sigma) \underset{\substack{\sigma\to\sigma_0 \\ \sigma<\sigma_0}}{\sim} \sqrt{2}D(\alpha)[\kappa(M_-\{\sigma_0, \sigma_0\}, \alpha, \alpha) + \kappa(M_+\{\sigma_0, \sigma_0\}, \alpha, \alpha)]$$

(B9)

$$\cdot \ln\left[\frac{3}{4}\left(\frac{\sigma_0}{\sigma}\right)^{1/2} + \frac{1}{4}\left(\frac{\sigma_0}{\sigma}\right)^{3/2} - 1\right] + O(1).$$

Use of the same assumptions and techniques leads to the following results for $S(\sigma)$ as σ_0 from the right,

$$S(\sigma) \underset{\substack{\sigma\to\sigma_0 \\ \sigma>\sigma_0}}{\sim} \sqrt{2}D(\alpha)[\kappa(M_-\{\sigma_0, \sigma_0\}, \alpha, \alpha) + \kappa(M_+\{\sigma_0, \sigma_0\}, \alpha, \alpha)]$$

(B10)

$$\cdot \ln \frac{\dfrac{\sigma}{\sigma_0} + 1}{\left|2\sqrt{\dfrac{\sigma}{\sigma_0}} - \dfrac{\sigma}{\sigma_0} - 1\right|} + O(1).$$

REFERENCES

[1] L. B. FELSEN AND N. MARCUVITZ *Radiation and Scattering of Waves*, Prentice-Hall, Englewood Cliffs, NJ, 1973.

[2] M. LIGHTHILL, *Waves in Fluids*. Cambridge University Press, CL3 Cambridge, 1978.

[3] O. M. PHILLIPS, *Dynamics of the Upper Ocean*. Cambridge University Press, Cambridge, 1969.

[4] W. J. PIERSON AND L. MOSKOWITZ, *A proposed spectral form for fully developed wind seas based on the similarity theory of S. A. Kitaigordskii*, J. Geophys. Res., 69 (1964), pp. 1262ff.

[5] W. PODNEY, *Measurement of fluctuating magnetic gradients originating from oceanic internal waves*, Science, 205 (1979), pp. 1381ff.

[6] M. SHINOZUKA AND C. M. JAN, *Digital simulation of random processes and its application*, J. Sound Vib., 25 (1972), pp. 111ff.